3D elastic wavefield tomography in the time domain

Lluis Guasch, Ivan Stekl, Adrian Umpleby, and Mike Warner, Imperial College London*

SUMMARY

Wavefield inversion tries to minimise the difference between real and modelled seismic data, which means that its success relies in the accuracy of the wave equation solver used in the process. Then, the wave equation solver should take elastic phenomena into account in order to compare its results with real field data. The purpose of our project was to develop a 3D wavefield tomography algorithm with an elastic wave equation solver in order to recover elastic properties. First formulations of the elastic inverse problem were published more than 20 years ago (Tarantola (1986); Mora (1987)), but only recently the computational resources needed to apply it to 3D have become available.

INTRODUCTION

Acoustic wavefield inversion has been widely used because of the highly accurate models it provides. To improve the quality of the inversion results, a more complete solution of the wave equation is required, and so must include elastic effects. The solver we have developed uses explicit time-stepping by finite differences that are 4^{th} order in space and 2^{nd} order in time, and it has been implemented in a tomographic algorithm.

Correlation of normal and shear stresses provide gradients for the V_p and V_s elastic parameters respectively. Since each set of parameters corresponds to a different shape of the objective function, the choice of parameters to invert can change the convergence rate of the inversion (Mora (1987)). For transmission tomography, the choice of V_p and V_s narrow the minima in the solution space, and we chose to invert these parameters. Obvious alternatives would be the Lame parameters, but further exploration of possible parameters to invert may lead to better behaved solution spaces. We show the results of our 3D elastic wavefield tomography code, and compare the outcome to that obtained inverting elastic data using a purely acoustic inversion algorithm.

In terms of computational resource, the elastic code is an order of magnitude more demanding than the equivalent acoustic code. We have combined shared memory with distributed memory parallelisation using openMP and MPI respectively. Thus, we take advantage of the increasingly common multicore architecture processors.

ELASTIC WAVEFIELD TOMOGRAPHY

Wavefield inversion aims to minimise the misfit between field and modelled data. Synhtetic seismograms are generated by solving the wave equation —using numerical methods— in a discretised space. When the difference between field and modelled data, known as misfit function, is below a certain threshold, we consider that the model used to model the synthetic data represents the real world. The inversion process consists of two major steps: generate synthetic data and update the model in the direction that minimises the misfit function. When we linearise the problem, assuming that we are near the absolute minimum in the solution space, the direction of the update can be calculated by correlating the forward wavefield and the backpropagated residuals (see for example, Pratt (1999)).

Forward modelling

The elastic wave equation can be written as a coupled system of equations:

$$\rho \frac{\partial \mathbf{v}}{\partial t} = \nabla \tau \tag{1}$$

$$\frac{\partial \tau}{\partial t} = \mathbf{c} : \nabla \tag{2}$$

where ρ is the density, $\mathbf{v}$ is the particle velocity vector, τ is the stress tensor, $\mathbf{c}$ is the elastic tensor and **:** denotes the Frobenius inner product. The stencil is staggered both in space and time and is based on the one developed by Levander (1988). The variables $\mathbf{v}$ and τ are distributed spatially as shown in Figure 1 and calculated at intermediate time-steps with respect to each other. Since the time operator is second order, only one array per variable is needed. To prevent spurious reflections from the boundaries we used an unsplit formulation of the Perfectly Matched Layers. We speeded up our modelling scheme by

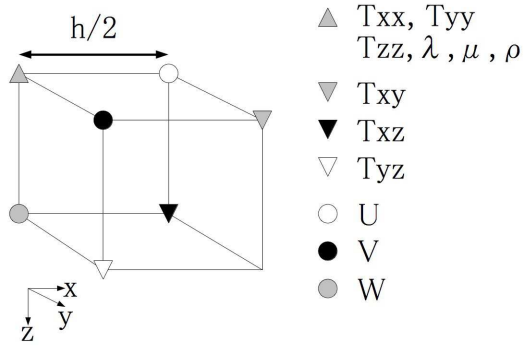

Figure 1: 3D unit cell used. Tii and Tij (i,j ∈ { x,y,z }) are the discrete normal and shear stresses respectively; λ and μ are the Lame parameters; U, V and W are the discrete particle velocities in x, y and z directions.

solving the FD equations in a sub-domain region around the source. We let this region grow as the wavefront evolves, until it reaches the model limits. Analogously, the information that can hit the receivers is confined in a shrinking box as time

increases. The intersection of these two boxes defines the subdomain where the wave equation is solved.

Inversion

The computational cost of wavefield tomography has prevented its 3D implementation for many years, and only recently has been applied thanks to modern hardware capabilities.

Direct application of the inverse problem formulation would imply an explicit calculation of the Frechet kernel (derivative of the wavefield with respect to the parameters) and this is still unaffordable. An alternative expression for the explicit derivative of the wavefield was developed by Tarantola (1986) where the problem is treated as a locally iterative linearised gradient descent method. Such approach is based on the propagation backwards in time of the difference between modelled and field data. In the acoustic approximation, the correlation between the forward modelled and the backpropagated pressure wavefields provides an expression for the V_p gradient, or in other words, provides the direction in which to update the model. Such approach has been used successfully in both 2D and 3D (Pratt (1999); Warner et al. (2007)). In the elastic case, we correlate normal and shear stress wavefields to calculate the P and S-wave velocity gradients respectively, as demonstrated below.

The misfit function has different shapes depending on the parameterisation of the model. The choice of parameters affects the shape of such function and, therefore, the convergence rate when we linearise it. We choose to update V_p and V_s instead of the Lam parameters because the minima are narrower for wide-angle geometries. Due to our wave equation formulation, which solves for particle velocities and stresses, we derive expressions for the P- and S-wave gradients in terms of the stresses rather than particle displacements. Shipp and Singh (2002) developed an expression for the P-wave gradient in terms of the normal stresses, which we have extended to the S-wave case. The expressions of the gradient in terms of the Lame parameters are of the form:

$$\delta\gamma = \int dt[\Omega^{\gamma}_{ijk}\overrightarrow{u}_j(\mathbf{x},t)][\Omega^{\gamma}_{ijk}\overleftarrow{\Psi}_j(\mathbf{x},t)] \tag{3}$$

where $\delta\gamma$ represents the gradient for $\gamma \in \{\lambda,\mu,\rho\}$, $\overrightarrow{u}_j$ is the j^{th} component of the forward propagated particle displacement wavefield, $\overleftarrow{\Psi}_j$ is the j^{th} component of the backpropagated residuals wavefield and Ω^{γ}_{ijk} is an operator with values:

$$\Omega^{\rho}_{ijk} = \sqrt{-1}\partial_t \tag{4}$$

$$\Omega^{\lambda}_{ijk} = \sqrt{-1}\partial_j \tag{5}$$

$$\Omega^{\mu}_{ijk} = \sqrt{\frac{-1}{2}}(\delta_{jk}\partial_i + \delta_{ji}\partial_k \tag{6}$$

The relation between $\{\lambda,\mu\}$ and $\{V_p,V_s\}$ gradients is given by:

$$\delta V_p = 2\rho V_p \delta\lambda \tag{7}$$

$$\delta V_s = 4\rho V_p \delta\lambda + 2\rho V_s \delta\mu \tag{8}$$

where we dropped $\delta\rho$ because we kept the density constant throughout the inversion process. Rewriting the equations (1) and (2) in terms of particle displacements instead of velocities gives us the following relationship between stresses and displacements (Einstein notation):

$$\frac{1}{\lambda+2\mu}\tau_{ii} = \frac{u_j}{j} \tag{9}$$

$$\frac{2-\delta_{ij}}{\delta_{ij}\lambda+\mu}\tau_{ij} = \frac{\partial u_i}{j} + \frac{\partial u_j}{i} \tag{10}$$

with $i,j \in \{x,y,z\}$. By combining equations (7-10) it is possible to write the gradient expressions in terms of stresses instead of particle displacements. As one may think intuitively, the correlation of the forward and backpropagated normal stresses provides the V_p gradient and the correlation of the shear stresses, the V_s gradient. The final gradient expressions are:

$$\delta V_p = \int dt(\overrightarrow{\tau_{xx}} + \overrightarrow{\tau_{yy}} + \overrightarrow{\tau_{zz}})(\overleftarrow{\tau_{xx}} + \overleftarrow{\tau_{yy}} + \overleftarrow{\tau_{zz}}) \tag{11}$$

$$\delta V_s = \int dt(\overrightarrow{\tau_{xy}} + \overrightarrow{\tau_{xz}} + \overrightarrow{\tau_{yz}})(\overleftarrow{\tau_{xy}} + \overleftarrow{\tau_{xz}} + \overleftarrow{\tau_{yz}}) \tag{12}$$

APPLICATION TO SYNTHETIC DATA

Two synthetic datasets were inverted. The first was generated using a 3D homogeneous cube with eight cubic anomalies, shown in Figure 2. The model was illuminated using plane P- and S-waves in two of the faces of the cube, and two planes of receivers were placed in the opposite faces.

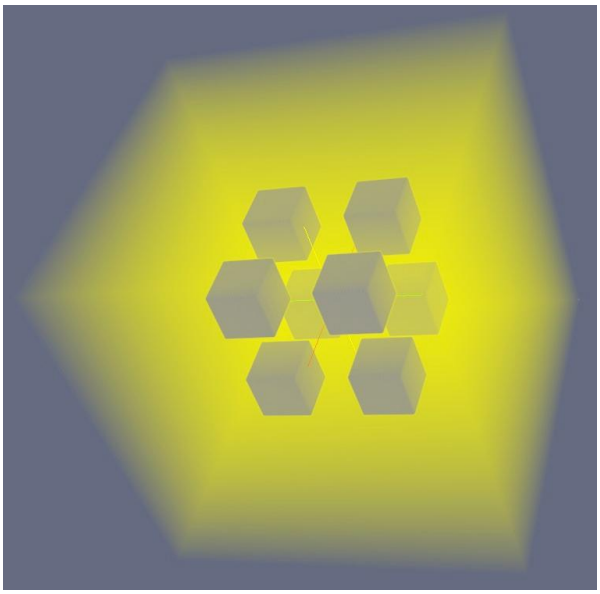

Figure 2: The dimensions of the model are 141x141x141 nodes. The elastic parameters are: background $V_p = 2500m/s$; background $V_s = 1443.4m/s$; anomalies $V_p = 2625m/s$; anomalies $V_s = 1515.5m/s$

Shear and normal stresses values are needed in order to calculate the gradients, but there is no need to store them at every single time-step. Taking into account that the source highest frequency was $10Hz$, we could store the two stress wavefields

every $\Delta t_{store} = 1/2f_N$, taking $f_N = 10Hz$ as the Nyquist frequency. Thus, only 60 time-steps are needed instead of the modelling original number of time-steps (454).

A homogeneous cube with V_p and V_s equal to the background was used as a starting model. Images of the gradients after one iteration push the model towards the minimum, as shown in Figure 4.

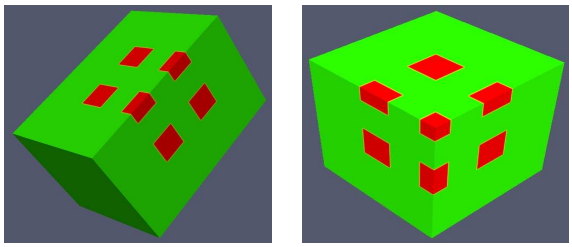

(a) (b)

Figure 3: Views of the eight cube model serve as a reference to assess the quality of the gradient images. **a)** True model showing the same cutaway as in Figure 6(a); **b)** Idem. for Figure 6(b)

A similar strategy was adopted for the second model, which has a shallow (high velocity anomaly) and a deep (low velocity anomaly) channel in a 1D velocity-gradient —ranging from $2000m/s$ to $3000m/s$— background. The dimensions of the model are 161x161x51 nodes. The 1D background velocity-gradient was used as a starting model. In this case, 30 time-steps were kept in memory to calculate the gradient. As in the previous case, we stored only a small number of the total 795 time-steps used during the forward modelling. The medium was illuminated with three plane wave sources placed in the top of the model. A P-wave —z direction— and two different S-wave sources —x and y directions. Figure 5 shows the starting and true models and Figure 6 shows the normalised V_p and V_s gradients after one iteration. The V_s gradient will update the shear velocities more accurately than the V_p gradient.

In both cases, a linear search was used to calculate the step-length.

CONCLUSIONS

We have developed a wavefield inversion algorithm that successfully recovers the elastic properties of the subsurface. The full elastic wave equation makes it possible to invert S-wave velocities, which have shorter wavelengths and thus can resolve smaller geological features.

ACKNOWLEDGMENTS

This work was sponsored by the FULLWAVE III consortium consisting of BIS, BG, BP, Chevron, CGGVeritas, ConocoPhillips, ENI, Maersk, Nexen, OHM, and Rio Tinto, under the ITF programme.

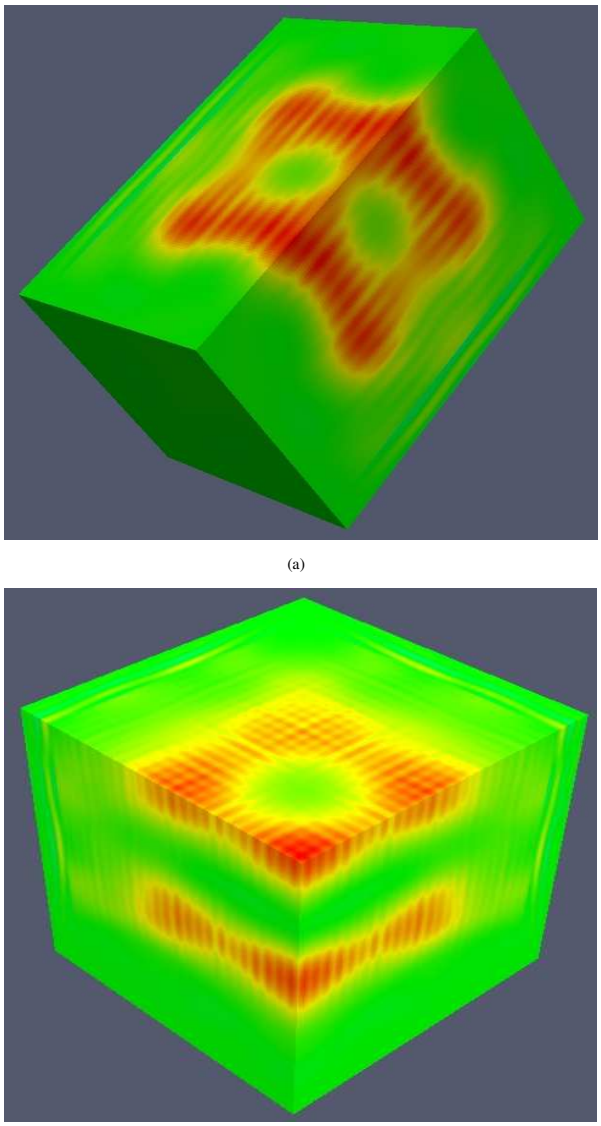

(a)

(b)

Figure 4: Normalised gradients after the first iteration obtained correlating normal stresses **(a)** and shear stresses **(b)**.

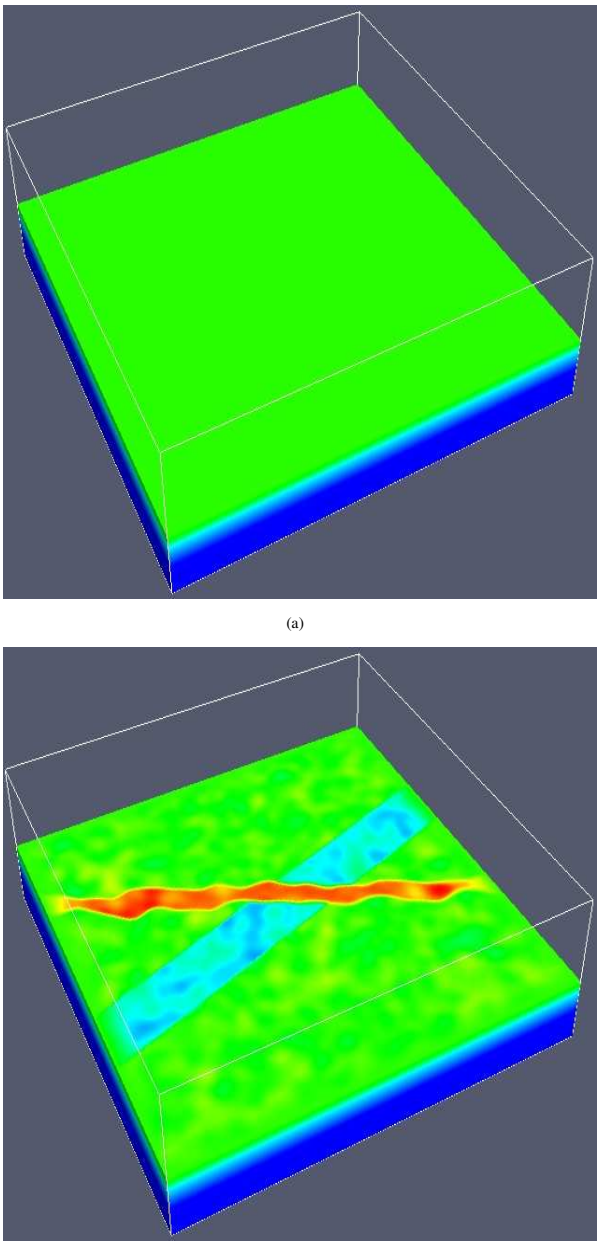

(a)

(b)

Figure 5: 3D view of the starting model **(a)** and the two channel model **(b)** used in the inversion.

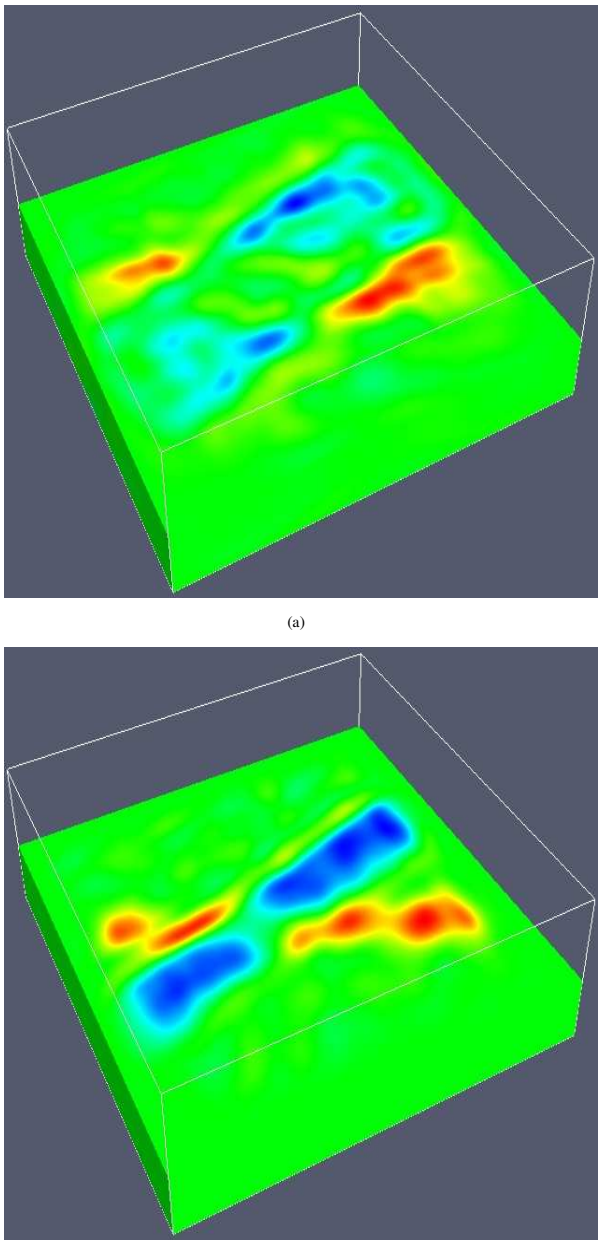

(a)

(b)

Figure 6: Gradients obtained correlating the stress fields show the direction in which to update the elastic parameters (seismic velocities in our case). Same point of view as in Figure 5 showing the V_p **(a)** and the V_s **(b)** normalised gradients.

EDITED REFERENCES

Note: This reference list is a copy-edited version of the reference list submitted by the author. Reference lists for the 2010 SEG Technical Program Expanded Abstracts have been copy edited so that references provided with the online metadata for each paper will achieve a high degree of linking to cited sources that appear on the Web.

REFERENCES

Levander, A., 1988, Fourth-order finite-difference P-SV seismograms: Geophysics, **53**, 1425, doi:10.1190/1.1442422.

Mora, P., 1987, Nonlinear two-dimensional elastic inversion of multioffset seismic data: Geophysics, **52**, 1211, doi:10.1190/1.1442384.

Pratt, R., 1999, Seismic waveform inversion in the frequency domain, Part 1: Theory and verification in a physical scale model: Geophysics, **64**, 888–901, doi:10.1190/1.1444597.

Shipp, R., and S. Singh, 2002, Two-dimensional full wavefield inversion of wide-aperture marine seismic streamer data: Geophysical Journal International, **151**, no. 2, 325–344, doi:10.1046/j.1365-246X.2002.01645.x.

Tarantola, A., 1986, A strategy for nonlinear elastic inversion of seismic reflection data: Geophysics, **51**, 1893–1903, doi:10.1190/1.1442046.

Warner, M., I. Stekl, and A. Umpleby, 2007, Full waveform seismic tomography-iterative forward modelling in 3D: 69th meeting, EAGE, Expanded Abstracts, C.